Molecular Spin Frustration in the $[Fe_4O_2]^{8+}$ Core: Synthesis, Structure, and Magnetochemistry of $[Fe_4O_2(O_2CR)_7(bpy)_2](ClO_4)$ (R = Me, Ph)

James K. McCusker,[†] John B. Vincent,[‡] Edward A. Schmitt,[†] Marion L. Mino,[‡] Koo Shin,[‡] DeAnna K. Coggin,[‡] Paula M. Hagen,[†] John C. Huffman,[§] George Christou,*[,‡] and David N. Hendrickson*[,†]

Contribution from the Department of Chemistry, 0506, University of California, San Diego, La Jolla, California 92093-0506, and the Department of Chemistry and the Molecular Structure Center, Indiana University, Bloomington, Indiana 47405. *Received July 19, 1990*

Abstract: The structural, spectroscopic, and magnetochemical characteristics of a new tetranuclear iron-oxo complex are reported. $[Fe_4O_2(O_2CCH_3)_7(bpy)_2](ClO_4)\cdot{}^1/_4CH_2Cl_2\cdot H_2O$ (**1**) crystallizes in the monoclinic space group $C2/c$ with a = 27.261 (10) Å, b = 11.789 (4) Å, c = 16.439 (5) Å, β = 118.27 (2)°, V = 4653.19 Å^3, and Z = 4. The structure was refined with 2646 reflections having $F > 2.33\sigma(F)$, giving final R factors of 0.0644 and 0.0688 for R and R_w, respectively. The $[Fe_4O_2]^{8+}$ core of the cation is structurally similar to other $[M_4O_2]^{8+}$ (M = Mn, Fe) complexes which have been previously reported. The core structure consists of a tetranuclear bis(μ_3-O) cluster disposed in a "butterfly" arrangement. Two different Fe–O(oxide) bridge distances of 1.819 (5) Å (wing–body) and 1.926 (5) Å (body–body) are observed. These differences are reflected in the Mössbauer spectrum of the complex, which analyzes as two quadrupole-split doublets in the range of 100–300 K. Each of the doublets has parameters characteristic of high-spin Fe(III) ions. ^{1}H NMR spectra are reported for two $[Fe_4O_2]^{8+}$ complexes. Assignments for all resonances were made on the basis of chemical shift data for two related complexes and one deuterated complex as well as measurements of spin–lattice (T_1) relaxation times. The magnetic susceptibility of complex **1** was measured in the range of 5.01–277.4 K. The effective moment per molecule decreases gradually from 4.20 μ_B at 277.4 K to 0.82 μ_B at 5.01 K, indicating a diamagnetic S = 0 ground state. A detailed theoretical analysis of the susceptibility data using a spin Hamiltonian approach gives a value for the "wing-body" Fe–Fe magnetic exchange interaction parameter of $J_{wb} = -45$ cm^{-1}. It was interesting to find that the "body–body" interaction J_{bb} is indeterminate and can only be described as being more positive than -15 cm^{-1}. The lack of definition of J_{bb} is due to spin frustration, where the relative magnitudes of the antiferromagnetic J_{wb} and J_{bb} interactions result in a net alignment of the spin vectors on the two body dioxo bridge core Fe^{III} ions. The significance of these results as they pertain to exchange coupling in iron–oxo proteins is discussed.

Introduction

The biological role of polynuclear oxo-, hydroxo-, and alkoxo-bridged iron systems has become a subject of considerable interest in the last few years.[1] Studies on various metalloproteins such as hemerythrin (Hr),[2] methane monooxygenase (MMO),[3] and ribonucleotide reductase[4] reveal that the active sites in all these systems likely contain (μ-oxo or μ-hydroxo)(μ-carboxylato)diiron cores, where the iron site can cycle from Fe_2^{II} to Fe_2^{III}. In view of the varied functions of these proteins (e.g., oxygen transport in Hr vs catalytic oxidation in MMO), the similarity in structure is quite remarkable. In addition, the iron storage protein ferritin (Ft) has received much attention for its role in the storage, detoxification, and recycling of iron in a wide range of biological systems.[5] Ft differs from the aforementioned protein systems in that it involves much larger aggregates of iron atoms. Hemosiderins (Hs) are probably similar to Ft, although little is known about the actual size of the polynuclear units in this protein.[6]

Synthetic efforts to prepare model complexes of this relatively new class of iron proteins have produced some interesting chemistry, in addition to providing some insight as to the possible factors controlling their function in biological systems. Attempts to prepare asymmetrically ligated binuclear model complexes for Hr by Lippard and co-workers[7] led instead to a novel tetranuclear molecule, $(Et_4N)[Fe_4O_2(O_2CR)_7(H_2B(pz)_2)_2]$, where $H_2B(pz)_2^-$ is the dihydrobis(1-pyrazolyl)borate anion. This molecule contains Fe(III) ions disposed in a "butterfly" $[Fe_4O_2]^{8+}$ core, where bridging between the iron ions occurs via two μ_3-O^{2-} anions. Six other tetranuclear Fe(III) complexes have been reported: two with this butterfly core structure[8] and four complexes containing μ_1-O(R) groups.[9]

A point of considerable interest is the nature of the magnetic exchange interactions in polynuclear iron complexes. By far the best characterized of exchange interactions in polynuclear iron complexes are those found in binuclear complexes. Lippard and Gorun have recently established an empirical relationship between

[†] University of California, San Diego.
[‡] Indiana University, Chemistry Department.
[§] Indiana University, Molecular Structure Center.

(1) (a) Lippard, S. J. *Angew. Chem., Int. Ed. Engl.* **1988**, *27*, 344. (b) Lippard, S. J. *Chem. Br.* **1986**, 222. (c) Que, L.; Scarrow, R. C. In *Metal Clusters in Proteins*; Que, L., Ed.; ACS Symposium Series 372; American Chemical Society: Washington, DC, 1988; Chapter 8.

(2) (a) Sheriff, S.; Hendrickson, W. A.; Smith, J. L. *J. Mol. Biol.* **1987**, *197*, 273. (b) Sheriff, S.; Hendrickson, W. A.; Smith J. L. *Life Chem. Rep. Suppl. Ser. 1* **1983**, 305. (c) Wilkins, P. C.; Wilkins, R. G. *Coord. Chem. Rev.* **1987**, *79*, 195–214.

(3) (a) Lund, J.; Woodland, M. P.; Dalton, H. *Eur. J. Biochem.* **1985**, *147*, 305. (b) Dalton, H. *Adv. Appl. Microbiol.* **1980**, *26*, 71. (c) Woodland, M. P.; Dalton, H. *J. Biol. Chem.* **1984**, *259*, 53. (d) Fox, B. G.; Surerus, K. K.; Münck, E.; Lipscomb, J. D. *J. Biol. Chem.* **1988**, *263*, 10553. (e) Ericson, A.; Hedman, B.; Hodgson, K. O.; Green, J.; Dalton, H.; Bentsen, J. G.; Beer, R. H.; Lippard, S. J. *J. Am. Chem. Soc.* **1988**, *110*, 2330.

(4) Averill, B. A.; Davis, J. C.; Burman, S.; Zirino, T.; Sanders-Loehr, J.; Loehr, T. M.; Sage, J. T.; Debrunner, P. G. *J. Am. Chem. Soc.* **1987**, *109*, 3760 and references cited therein. (b) A preliminary X-ray structure has been reported: Nordlund, P.; Sjöberg, B.-M.; Eklund, H. *Nature* **1990**, *345*, 593–598.

(5) (a) Theil, E. C. *Annu. Rev. Biochem.* **1987**, *56*, 289. (b) Ford, G. C.; Harrison, D. M.; Rice, D. W.; Smith, J. M. A.; Treffry, A.; White, J. L.; Yariv, J. *Philos. Trans. R. Soc. London Ser. B* **1984**, *304*, 551. (c) Crichton, R. R. *Angew. Chem., Int. Ed. Engl.* **1973**, *12*, 57.

(6) (a) Mann, S.; Bannister, J. V.; Williams, R. J. P. *J. Mol. Biol.* **1986**, *188*, 225. (b) Ford, G. C.; Harrison, P. M.; Rice, D. W.; Smith, J. M. A.; Treffry, A.; White, J. L.; Yariv, J. *Rev. Port. Quim.* **1985**, *27*, 119. (c) Smith, J. M. A.; Helliwell, J. R. *Inorg. Chem. Acta* **1985**, *106*, 193. (d) Theil, E. C. *Adv. Inorg. Biochem.* **1983**, *5*, 1, and references cited therein.

(7) Armstrong, W. H.; Roth, M. E.; Lippard, S. J. *J. Am. Chem. Soc.* **1987**, *109*, 6318.

(8) (a) Ponomarev, V. I.; Atovmyan, L. O.; Bobkova, S. A.; Turtē, K. I. *Dokl. Akad. Nauk. SSSR* **1984**, *274*, 368. (b) Gorun, S. M.; Lippard, S. J. *Inorg. Chem.* **1988**, *27*, 149. (c) Stukan, R. A.; Ponomarev, V. I.; Nifontov, V. P.; Turtē, K. I.; Atovmyan, L. D. *J. Struct. Chem.* **1985**, *26*, 197.

(9) (a) Drüeke, S.; Wieghardt, K.; Nuber, B.; Weiss, J.; Bominar, E. L.; Sawaryn, A.; Winkler, H.; Trautwein, A. X. *Inorg. Chem.* **1989**, *28*, 4477. (b) Chen, Q.; Lynch, J. B.; Gomez-Romero, P.; Ben-Hussien, A.; Jameson, G. B.; O'Connor, C. J.; Que, L., Jr. *Inorg. Chem.* **1988**, *27*, 2673. (c) Jameson, D. L.; Xie, C.-L.; Hendrickson, D. N.; Potenza, J. A.; Schugar, H. L. *J. Am. Chem. Soc.* **1987**, *109*, 740. (d) Murch, B. P.; Boyle, P. D.; Que, L., Jr. *J. Am. Chem. Soc.* **1985**, *107*, 6728.

0002-7863/91/1513-3012$02.50/0

the strength of magnetic exchange and the shortest distance of superexchange pathway for binuclear Fe(III) complexes.[10] However, there are few detailed magnetochemistry studies on complexes of higher nuclearity. This is due to the increased complexity involved with carrying out theoretical treatments of large spin systems. Both Drüke et al.[9a] and Jameson et al.[9c] have performed theoretical analyses on data for μ_1-O bridges, but as yet there has been no published attempt at analyzing the magnetic characteristics of molecules possessing the butterfly $[Fe_4O_2]^{8+}$ core.

Our recent success with the synthesis and characterization of tetranuclear manganese complexes having the formulation $Mn_4O_2(O_2CCH_3)_6(bpy)_2$ and $[Mn_4O_2(O_2CR)_7(bpy)_2]^{z+}$ (z = 1 for four Mn(III))[11] prompted us to extend this work to analogous Fe/RCO_2^-/bpy complexes with the $[Fe_4O_2]^{8+}$ core. We herein report the successful preparation of compounds containing the $[Fe_4O_2(O_2CR)_7(bpy)_2]^+$ cation and compare their structures and spectroscopic characteristics to the analogous Mn(III) complexes. In addition, the results of a detailed magnetochemical study are reported which reveal some unexpected results regarding the extent and nature of the exchange interactions involved in this class of polynuclear Fe(III) complexes.

Experimental Section

All manipulations were performed under anaerobic conditions with use of materials as received. MeCN and absolute EtOH were stored over molecular sieves; other solvents were not purified unless indicated. CD_3CO_2D (99.5% D) was obtained from Aldrich. **Warning: Appropriate care should be taken in the use of ClO_4^- salts. The described compounds have not displayed any explosive tendencies, but caution is advised.**

$[Fe_4O_2(O_2CCH_3)_7(bpy)_2](ClO_4)\cdot{}^1/_4CH_2Cl_2\cdot H_2O$ (1). Method A. A stirred orange solution of $FeCl_3\cdot 6H_2O$ (7.21 g, 26.7 mmol) in EtOH (150 mL) was treated with solid NaOAc (5.44 g, 66.3 mmol) and bpy (2.23 g, 14.3 mmol). After stirring for 15 min, $NaClO_4$ (4.09 g, 33.4 mmol) was added to the brown reaction mixture, and the resulting green-brown slurry was stirred overnight at ambient temperature. A fine green solid was collected by filtration, washed with copious amounts of EtOH and Et_2O, and dried in air. The solid was extracted with CH_2Cl_2 (125 mL) and filtered, and the filtrate was layered with an equal volume of hexanes. After several days, the resulting dark green-brown crystals were collected by filtration, washed with hexanes, and air-dried; the yield was 60%. The crystallographic sample was taken at this point. The bulk material was recrystallized from CH_2Cl_2/hexanes and analyzed. Anal. Calcd for $C_{34.25}H_{39.5}N_4O_{21}Cl_{1.5}Fe_4$: C, 36.74; H, 3.56; N, 5.00; Cl, 4.75; Fe, 19.95. Found: C, 36.42; H, 3.42; N, 4.88; Cl, 4.80; Fe, 19.9. This sample provided the material for the magnetochemical studies.

$[Fe_2OCl_2(bpy)_4](ClO_4)_2\cdot MeCN$ (2). The light green solid residue remaining from the CH_2Cl_2 extraction above was dissolved in MeCN (50 mL) and filtered to remove some white solid. The brown filtrate was allowed to concentrate by slow evaporatioin to give large brown crystals of a second product, $[Fe_2OCl_2(bpy)_4](ClO_4)_2$ (**2**), in 10% yield. IR 2240 (m), 1590 (m), 1315 (s), 1245 (m), 1220 (m), 1175 (m), 1160 (m), 1090 (vs, br), 1020 (m), 1010 (m), 820 (vs, br), 760 (s), 730 (s), 650 (m), 615 (s), 410 (m). Anal. Calcd for $C_{42}H_{35}N_9O_4Cl_4Fe_2$: C, 47.44; H, 3.32; N, 11.86; Cl, 13.34; Fe, 10.50. Found: C, 47.5; H, 3.4; N, 12.0; Cl, 12.8; Fe, 10.2.

Method B (for 1). A stirred solution of $Fe(ClO_4)_3\cdot 6H_2O$ (8.64 g, 18.7 mmol) in EtOH (100 mL) was treated with solid NaOAc (2.57 g, 31.3 mmol) and bpy (1.17 g, 7.5 mmol) to produce a dark brown solution. After 0.5 h of stirring, a precipitate began to form, and after overnight stirring, a thick green-brown slurry was obtained. The solid was collected by filtration, extracted with CH_2Cl_2, and layered with hexanes, as described in method A. Pure green-brown crystals were obtained after this one layering; the yield was 65%. As anticipated from the absence of Cl^- in the reaction mixture, complex **2** was not obtained from method B. The analytical data suggested a slightly different formulation, **1**·$^1/_2CH_2Cl_2\cdot H_2O$. Electronic absorption spectrum in MeCN λ_{max}, nm (ϵ_M/Fe$_4$, M^{-1} cm^{-1}) 234 (49 300), 284 (29 360), 304 (sh, 21 410), 334 (sh, 11 260), 404 (sh, 3090), 466 (1670), 568 (sh, 270); IR 1609 (m), 1584 (vs, br), 1564 (s), 1555 (sh), 1447 (vs, br), 1414 (s, br), 1347 (m), 1316 (w), 1095 (s, br), 1026 (s), 772 (m), 737 (m), 706 (m), 658 (s), 625 (m), 560 (w), 495 (w). Anal. Calcd for $C_{34.5}H_{40}N_4O_{21}Cl_2Fe_4$: C, 36.32; H, 3.53; N, 4.91; Fe, 19.58. Found: C, 36.26; H, 3.29; N, 4.74; Fe, 19.48.

The $CD_3CO_2^-$ version of complex **1** was prepared in a similar fashion. NaO_2CCD_3 was prepared in situ by adding Na metal (1.22 g, 53.0 mmol) to EtOH (30 mL) and adding CD_3CO_2D (3.0 mL, 532 mmol). This solution was added in place of NaOAc in the procedure above. The crude product was recrystallized twice from CH_2Cl_2/hexanes; the yield was 70%.

$[Fe_4O_2(O_2CCH_3)_7(4,4'\text{-}Me_2bpy)_2](ClO_4)\cdot 2H_2O$ (3). Method B for complex **1** was repeated by using 4,4′-Me_2-2,2′-bipyridine (1.38 g, 7.50 mmol) in place of bpy. The crude material was recrystallized four times from CH_2Cl_2/hexane layerings before green-brown crystals of acceptable purity were obtained; the yield was 55%. Electronic spectrum in MeCN 284 (35 600), 340 (14 100), 408 (2990), 464 (1670), 584 (250); IR 1615 (m), 1593 (s, br), 1450 (vs, br), 1345 (m), 1319 (w), 1094 (s, br), 1026 (m), 924 (w), 835 (w), 698 (m), 663 (s), 621 (m), 559 (w), 523 (w). Anal. Calcd for $C_{38}H_{49}N_4O_{22}ClFe_4$: C, 38.90; H, 4.21; N, 4.78; Fe, 19.05. Found: C, 38.44; H, 4.01; N, 4.45; Fe, 19.71.

$[Fe_4O_2(O_2CPh)_7(bpy)_2](ClO_4)$ (4). Method A. To a stirred solution of $FeCl_3\cdot 6H_2O$ (3.50 g, 12.9 mmol) in EtOH (90 mL) were added NaO_2CPh (3.74 g, 26.0 mmol) and bpy (2.05 g, 13.1 mmol). After 15 min, $NaClO_4$ (1.60 g, 13.0 mmol) was added, and the reaction mixture was stirred overnight. The resulting green slurry was filtered, and the solid was washed with EtOH and Et_2O. The solid was extracted with CH_2Cl_2 (60 mL) and filtered, and the green-brown filtrate was layered with hexanes. The resulting brown crystals were recrystallized again from CH_2Cl_2/hexane to give brown needles; the yield was 30%. The material analyzed as **4**·$^3/_4CH_2Cl_2$. Anal. Calcd for $C_{69.75}H_{52.5}N_4Cl_{2.5}O_{20}Fe_4$: C, 53.06; H, 3.4; N, 3.5; Cl, 5.6; Fe, 14.1. Found: C, 52.55; H, 3.3; N, 4.2; Cl, 5.0; Fe, 14.0.

Method B. To a stirred solution of $Fe(ClO_4)_3\cdot 6H_2O$ (8.64 g, 18.7 mmol) in EtOH (100 mL) were added NaO_2CPh (4.51 g, 31.3 mmol) and bpy (1.17 g, 7.50 mmol). The reaction mixture was stirred overnight during which time a green-brown slurry was obtained. All subsequent manipulations were as in method A. The crude material was recrystallized twice from CH_2Cl_2/hexane layerings; the yield was 65%. The crystals analyzed as **4**·$^1/_2CH_2Cl_2$. Electronic spectrum in MeCN 284 (54 090), ~302 (sh, 37 620), 344 (sh, 14 800), ~406 (sh, 3500), 466 (1790), ~568 (sh, 300); IR 1599 (s), 1557 (s), 1532 (s), 1447 (s), 1397 (vs, br), 1376 (w), 1099 (s, br), 1026 (m), 771 (w), 719 (s), 675 (m), 625 (w), 524 (w), 476 (s). Anal. Calcd for $C_{69.5}H_{52}N_4Cl_2O_{20}Fe_4$: C, 53.60; H, 3.37; N, 3.60; Fe, 14.34. Found: C, 53.32; H, 3.20; N, 3.57; Fe, 13.91.

Method C. Treatment of **1** (0.27 g, 0.23 mmol) in CH_2Cl_2 (20 mL) with $PhCO_2H$ (0.45 g, 3.7 mmol) followed by equivolume addition of hexanes precipitates a yellow-brown solid of **4** in 60% yield; the spectroscopic data are identical with those of the authentic material.

Physical Measurements. Infrared (Nujol mull) and solution electronic spectra were recorded on Nicolet 510P FTIR and Hewlett-Packard Model 8450A spectrophotometers, respectively. ^{1}H NMR spectra were recorded on a Varian XL-300 spectrometer; chemical shifts are quoted on the δ scale (shifts downfield are positive) with the protio solvent signal as a reference. Elemental analyses were performed at the Microanalytical Laboratory, Department of Chemistry, Manchester University, England.

^{57}Fe Mössbauer Spectroscopy. Variable-temperature Mössbauer spectra were obtained by using a constant acceleration vertical drive spectrometer described previously.[12] The sample temperature was controlled by using a Lake Shore Cryogenics Model DRC80C temperature controller in conjunction with a Si diode mounted on the copper sample holder. The absolute accuracy is estimated at ±3 K. The spectra were fit to Lorentzian line shapes by using a modified version of a previously reported computer program.[13] Isomer shift values are reported relative to iron foil at 300 K and have not been corrected for the temperature-dependent second-order Doppler shift.

Magnetic Susceptibility. Magnetic susceptibility measurements from 5 to 280 K were performed by using a Model VTS-900 SQUID susceptometer (BTi, Inc., San Diego, CA). Temperature control was achieved by using a BTi digital temperature control device. All data were collected in an applied field of 10.0 kG. Diamagnetic corrections were estimated from Pascal's constants.[14] The effective magnetic moment of the complex was fit to the theoretical equation (vide infra) by using a relative error-fitting computer program.[15]

X-ray Crystallography. Data were collected for complex **1** on a Picker four-circle diffractometer employing an approximately equidimensional crystal (~0.25 mm); details of the diffractometry, low-temperature facilities, and computational procedures employed by the Molecular Structure Center are available elsewhere.[16] Crystallographic data are collected in Table I. A systematic search of a limited hemisphere of reciprocal space located a set of diffraction maxima with symmetry and

(10) Gorun, S. M.; Lippard, S. J. *Recl. J. R. Neth. Chem. Soc.* **1987**, *106*, 417.

(11) (a) Vincent, J. B.; Christmas, C.; Chang, H.-R.; Li, Q.; Boyd, P. D. W.; Huffman, J. C.; Hendrickson, D. N.; Christou, G. *J. Am. Chem. Soc.* **1989**, *111*, 2086. (b) Libby, E.; Schmitt, E. A.; McCusker, J. K.; Webb, R. J.; Folting, K.; Huffman, J. C.; Hendrickson, D. N.; Christou, G., submitted for publication.

systematic absences corresponding to the centered monoclinic space group $C2/c$. Subsequent successful refinement of the structure confirmed this assignment. The structure was solved by a combination of direct methods (MULTAN) and Fourier techniques and refined by a full-matrix least-squares approach. All non-hydrogen atoms of the cation were readily located and refined with anisotropic thermal parameters. The oxygen atoms of the ClO_4^- showed considerable disorder. A total of nine oxygen peaks with anisotropic thermal parameters were included in the latter refinement cycles; their relative occupancy factors were allowed to vary, with final refinement leading to occupancy factors in the range of 15–30%. Due to the severe disorder of the ClO_4^-, no attempt to locate or include solvent molecules or H atoms in the final refinement was made.

Results and Discussion

Syntheses. The first example of an Fe_4O_2/RCO_2^- complex, $[Fe_4O_2(O_2CCF_3)_8(H_2O)_6]$, was reported in 1984.[8a] This was followed by a handful of reports of other Fe_4O_2 complexes,[7,8b,9] so there was every reason to believe that stable Fe_4O_2/RCO_2^-/bpy complexes should be synthetically feasible if the correct procedures could be discovered. In our manganese chemistry, the lack of many readily available sources of Mn(III) led us to employ preformed $[Mn_3O(O_2CR)_6L_3]$ reagents in reactions with bpy. For the present iron chemistry it was considered much more convenient to employ $FeCl_3 \cdot 6H_2O$, at least until such time as an alternative approach became necessary. In fact, this initial approach proved successful. Reaction mixtures consisting of $FeCl_3$, NaOAc, and bpy in EtOH resulted in brown solutions from which a green precipitate forms on addition of $NaClO_4$. This solid was found to consist of two components, the desired $[Fe_4O_2(O_2CCH_3)_7(bpy)_2](ClO_4)$ (**1**) and the known compound $[Fe_2OCl_2(bpy)_4](ClO_4)_2$ (**2**).[17] The two materials were separated by their differing solubilities in CH_2Cl_2, although repeated recrystallization of **1** from CH_2Cl_2/hexanes is necessary to remove final traces of **2**. The ~2:1 Fe/bpy ratio in the procedure described above (method A) gives a good yield of **1** while keeping the yield of **2** low. A ratio of 1:1 results in **2** as the major product.

In seeking to prevent all formation of **2**, the Fe/bpy ratio was not increased further, but instead all sources of Cl^- were removed from the reaction. Use of $Fe(ClO_4)_3 \cdot 6H_2O$ in place of $FeCl_3 \cdot 6H_2O$ (method B) proved successful, and complex **1** was the sole product. This improved procedure was also employed for the preparation of the $CD_3CO_2^-$ version of **1** and also for the 4,4′-Me_2bpy analogue (**3**), although the latter needed several recrystallizations before analytical purity was achieved.

The two methods which lead to complex **1** can also be employed for the R = Ph derivative, complex **4**. Method A was only attempted for a 1:1 Fe/bpy ratio, so the yield of **4** was consequently low (~30%). However, the improved procedure (method B) satisfactorily gives higher isolated yields of pure material (65%). A third synthetic route to **4** is provided by a ligand substitution reaction of **1** with excess $PhCO_2H$. This procedure is based on the previously established conversion of $[Mn_4O_2(O_2CCH_3)_7(bpy)_2]^+$ to $[Mn_4O_2(O_2CPh)_7(bpy)_2]^+$ with the more acidic $PhCO_2H$. This substitution can be summarized by eq 1.

$$[Fe_4O_2(O_2CCH_3)_7(bpy)_2]^+ + 7PhCO_2H \rightarrow [Fe_4O_2(O_2CPh)_7(bpy)_2]^+ + 7CH_3CO_2H \quad (1)$$

The analytical data for the Fe_4O_2 complexes **1** and **4** suggest the presence of variable amounts of CH_2Cl_2 as solvates of crystallization. We believe that the crystals slowly lose CH_2Cl_2 and in some cases are also hygroscopic. The presence of CH_2Cl_2 in the solids was evident from the NMR spectra (vide infra), and the presence of H_2O was observed as a weak, broad feature in the IR at ~3450 cm^{-1}.

Description of Structure. An ORTEP plot of the cation of complex **1** is provided in Figure 1; selected metric parameters are collected in Table III. Complex **1** crystallizes in the monoclinic space group $C2/c$. The cation is positioned on a crystallographic 2-fold rotation axis. The asymmetric unit thus consists of half of the cation and a well-separated ClO_4^-, the central Cl atom having an occupancy factor of 0.5. As mentioned in the Experimental Section, the ClO_4^- oxygen atoms are severely disordered, preventing any attempt to locate the solvate molecules.

Table I. Crystallographic Data for $[Fe_4O_2(O_2CCH_3)_7(bpy)_2](ClO_4)\cdot{}^1/_4CH_2Cl_2\cdot H_2O$ (**1**)

formula[a]	$C_{34}H_{39}N_4O_{20}ClFe_4$
M_r, g mol^{-1}	1080.55
space group	monoclinic, $C2/c$
temp, °C	−155
a, Å	27.261 (10)
b, Å	11.789 (4)
c, Å	16.439 (5)
β, deg	118.27 (2)
V, Å^3	4653.19
Z	4
ρ_{calc}, g cm^{-3}	1.543
range collcd	$6° \le 2\theta \le 45°$
total data	5448
unique data	3048
averaging R^b	0.036
obsd data	2646 ($F > 2.33\sigma(F)$)
no. of refined variables	365
R (R_w), %	6.44 (6.88)

[a] Excluding solvent molecules. [b] For reflections measured more than once.

Table II. Fractional Coordinates and Isotropic Thermal Parameters for $[Fe_4O_2(O_2CCH_3)_7(bpy)_2](ClO_4)\cdot{}^1/_4CH_2Cl_2\cdot H_2O$ (**1**)[a]

atom	x/a	y/b	z/c	B_{iso}
Fe(1)	4114.6 (4)	1759 (1)	633 (1)	21
Fe(2)	4577.1 (4)	2652 (1)	2778 (1)	23
O(3)	4615 (2)	2539 (4)	1641 (3)	22
N(4)	3905 (3)	3060 (5)	9608 (4)	26
C(5)	4130 (4)	4110 (7)	9826 (6)	35
C(6)	4043 (4)	4897 (8)	9129 (7)	43
C(7)	3736 (4)	4579 (9)	8217 (7)	45
C(8)	3504 (4)	3492 (8)	8004 (6)	39
C(9)	3599 (3)	2745 (7)	8709 (5)	27
C(10)	3376 (3)	1576 (7)	8558 (5)	29
C(11)	3039 (4)	1135 (9)	7689 (6)	43
C(12)	2839 (4)	10023 (10)	7612 (7)	50
C(13)	2980 (4)	9424 (9)	8379 (8)	50
C(14)	3329 (3)	9901 (7)	9268 (6)	36
N(15)	3526 (3)	965 (5)	9332 (4)	26
O(16)	3432 (2)	2224 (5)	772 (4)	28
C(17)	3369 (3)	2694 (7)	1404 (6)	29
O(18)	3756 (2)	2973 (5)	2175 (4)	31
C(19)	2790 (4)	2969 (12)	1215 (8)	68
O(20)	4156 (2)	304 (4)	1266 (4)	26
C(21)	4262 (3)	163 (7)	2103 (6)	26
O(22)	4396 (2)	921 (4)	2696 (4)	26
C(23)	4218 (4)	8955 (7)	2377 (7)	43
O(24)	4697 (2)	1333 (4)	226 (3)	24
C(25)	5129 (3)	1857 (6)	355 (5)	21
O(36)	4616 (2)	2584 (5)	4024 (4)	29
C(27)	5359 (4)	1634 (8)	9694 (7)	43
O(28)	4693 (2)	4369 (5)	2786 (4)	32
C(29)	5000*	4840 (10)	2500*	41
C(30)	0*	1148 (12)	2500*	84
Cl(31)	2033 (3)	1610 (5)	4866 (4)	54
O(32)	7838 (21)	2004 (45)	786 (21)	53
O(33)	6516 (20)	4380 (25)	9127 (26)	68
O(34)	7413 (11)	4994 (21)	266 (20)	19
O(35)	3251 (25)	3141 (36)	4644 (56)	68
O(36)	7757 (13)	270 (31)	9759 (24)	77
O(37)	1483 (19)	1794 (51)	4540 (42)	73
O(38)	1954 (19)	737 (53)	5077 (31)	125
O(39)	6268 (9)	3882 (26)	9042 (15)	27
O(40)	2518 (42)	2598 (39)	4325 (24)	179

[a] Fractional coordinates are ×10^4 for non-hydrogen atoms and ×10^3 for hydrogen atoms. B_{iso} values are ×10. Isotropic values for those atoms refined anisotropically are calculated by using the formula given by Hamilton (Hamilton, W. C. *Acta Crystallogr.* **1959**, *12*, 609). Parameters marked by an asterisk (*) were not varied.

The cation of **1** lies in a 2-fold rotation axis perpendicular to the central Fe_2O_2 rhomboid, passing through C29 and C30 of the unique bridging $^-O_2CCH_3$ group. The cation possesses a $Fe_4(\mu_3\text{-}O)_2$ core with the four Fe(III) ions disposed in a "butterfly" arrangement, with each μ_3-O bridging a "wing". The core can

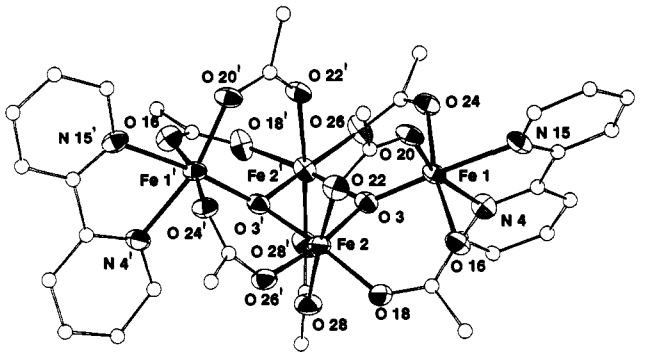

Figure 1. ORTEP plot of the $[Fe_4O_2(O_2CCH_3)_7(bpy)_2]^+$ cation of complex **1**.

Table III. Selected Bond Distances (Å) and Angles (deg) for $[Fe_4O_2(O_2CCH_3)_7(bpy)_2](ClO_4)\cdot{}^1/_4CH_2Cl_2\cdot H_2O$ (**1**)

	(a) Bonds		
Fe1–Fe1′	5.738 (4)	Fe1–N15	2.185 (6)
Fe1–Fe2	3.306 (4)	Fe2–O3	1.926 (5)
Fe1–Fe2′	3.439 (4)	Fe2–O3′	1.947 (5)
Fe2–Fe2′	2.855 (4)	Fe2–O18	2.010 (5)
Fe1–O3	1.819 (5)	Fe2–O22	2.090 (5)
Fe1–O16	2.054 (5)	Fe2–O26′	2.001 (5)
Fe1–O20	1.983 (5)	Fe2–O28	2.047 (6)
Fe1–O24	2.057 (5)		
Fe1–N4	2.145 (6)		
	(b) Angles		
O3–Fe1–O16	95.27 (22)	O3–Fe2–O3′	84.45 (22)
O3–Fe1–O20	97.30 (21)	O3–Fe2–O18	95.36 (22)
O3–Fe1–O24	93.34 (21)	O3′–Fe2–O18	173.10 (22)
O3–Fe1–N4	99.22 (23)	O3′–Fe2–O22	98.20 (20)
O3–Fe1–N15	173.82 (23)	O3–Fe2–O22	89.36 (20)
O16–Fe1–O20	90.01 (21)	O3–Fe2–O26′	171.68 (21)
O16–Fe1–O24	168.97 (21)	O3′–Fe2–O26′	89.73 (22)
O16–Fe1–N4	88.81 (23)	O3–Fe2–O28	89.76 (21)
O16–Fe1–N15	86.50 (22)	O3′–Fe2–O28	85.94 (21)
O20–Fe1–O24	95.73 (20)	O18–Fe2–O22	88.69 (22)
O20–Fe1–N4	163.49 (23)	O18–Fe2–O26′	91.14 (21)
O20–Fe1–N15	88.61 (23)	O18–Fe2–O28	87.16 (23)
O24–Fe1–N4	83.01 (22)	O22–Fe2–O26′	85.59 (21)
O24–Fe1–N15	84.24 (21)	O22–Fe2–O28	175.67 (22)
N4–Fe1–N15	74.88 (24)	O26′–Fe2–O28	95.75 (22)

be considered as two edge-sharing Fe_3O triangular units with the oxygen atoms slightly below the Fe_3 planes (as viewed in Figure 1). Peripheral ligation is provided by seven bridging $^-O_2CCH_3$ and two terminal chelating bpy groups, resulting in a distorted octahedral geometry about each Fe(III) site. The two "hinge" or "body" Fe atoms (Fe2 and Fe2′) are bridged by two oxides, whereas the wing-tip ions have only a single oxide bridge (in addition to the OAc^- groups). Consequently, the central Fe2···Fe2′ separation is much shorter than the body-to-wing separations (2.855 vs 3.306 and 3.439 Å, respectively). The μ_3-O atoms bridge somewhat asymmetrically, Fe1–O3 being noticeably shorter (1.819 (5) Å) than Fe2–O3 (1.926 (5) Å) and Fe2–O3′ (1.947 (5) Å). The short Fe1–O3 distance leads to a small trans influence on the Fe1–N15 bond (2.185 (6) Å), lengthening it relative to Fe1–N4 (2.145 (6) Å), but the difference is almost within 3σ. The asymmetry in the Fe···Fe and Fe–O distances within the Fe_3O units is also reflected in the Fe–O–Fe angles: Fe2–O3–Fe2′ is only 95.00 (22)°, whereas Fe1–O3–Fe2 [123.91 (26)°] and Fe1–O3–Fe2′ [131.90 (27)°] are significantly larger.

The $Fe_4(\mu_3\text{-}O)_2$ core found in the cation of complex **1** is also found in $[Fe_4O_2(O_2CCF_3)_8(H_2O)_6]$[8a] $[Fe_4O_2(bicoh)_2(bico)_2(O_2CPh)_4]Cl_2$[8b] (bicoh = bis(*N*-methylimidazol-2-yl)carbinol), and $(NEt_4)[Fe_4O_2(O_2CPh)_7(H_2B(pz)_2)_2]$ ($H_2B(pz)_2$ = dihydrobis(1-pyrazolyl)borate).[7] In the first two complexes, the $[Fe_4O_2]^{8+}$ core has a planar disposition of the metal atoms; only the third complex has the bent "butterfly" structure exhibited by **1**. Gorun and Lippard have carried out detailed analyses of the core geometries in both the planar and butterfly structural types.[8b] A summary of their results as compared to what is found for complex **1** is given in Table IV. In describing the geometry of the tetrairon core, Gorun and Lippard examined the distances and angles defined below.

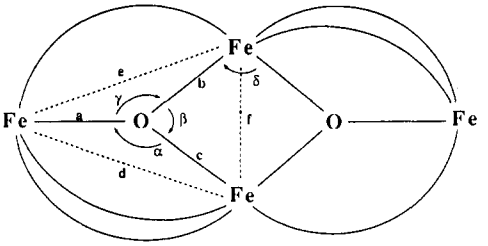

It is clear from an examination of Table IV that the structural parameters for **1** fall in the range reported for the other $[Fe_4O_2]^{8+}$ complexes. In particular for the two nonplanar butterfly structures (**1** and ref 7), the $[Fe_4O_2]^{8+}$ cores are almost completely superimposable. Detailed comparisons for the previously reported $[Fe_4O_2]^{8+}$ complexes may be found elsewhere.[1a,8b]

^{57}Fe Mössbauer Spectroscopy. Mössbauer spectra for complex **1** were collected as a function of temperature between 105 and 300 K, see Figure 2. Each spectrum is best fit to two equal-area doublets, in accord with the symmetry of the tetranuclear core. The isomer shifts (δ) for both doublets are similar, falling in the range of 0.45–0.49 mm/s with little temperature dependence, see Table V. These values for δ are within the range expected for a high-spin Fe(III) ion. The two doublets do, however, exhibit differences in ΔE_Q: for one doublet, ΔE_Q varies from 0.962 (4) mm/s at 105 K to 0.916 (12) mm/s at 300 K, whereas the second signal has a larger value (1.333 (3) mm/s at 105 K, 1.293 (10) mm/s at 300 K). The ΔE_Q values for both sites reflect deviations from octahedral coordination geometry at each site, since the valence electron contribution to ΔE_Q is negligible for a high-spin Fe(III) ion. In particular, the N_2O_4 coordination sphere about Fe(1) exhibits bond distances varying from 1.819 (5) Å for Fe(1)–O(3) to 2.185 (5) Å for Fe(1)–N(15). The more symmetric O_6 coordination sphere about Fe(2), possessing both of the longer Fe–$O_{\mu 3}$ bonds, encompasses a more restricted bond length range of 1.926 (4)–2.090 (5) Å. The Fe(2) signal is therefore assignable to the doublet with $\Delta E_Q < 1$ mm/s, whereas Fe(1) shows a larger ΔE_Q due to the asymmetric ligation and short Fe(1)–O(3) bond and is assigned as the outer doublet. In their study of butterfly $[Fe_4O_2]^{8+}$ complexes, Armstrong et al.[7] noted a correlation of difference in ΔE_Q for body vs wing Fe(III) ions with the length of the Fe–(μ_3-oxo) bond at the two iron sites in each complex. For $(Et_4N)[Fe_4O_2(O_2CPh)_7(H_2B(pz)_2)_2]$ they observed only one doublet with ΔE_Q = 1.21 mm/s at 80 K, whereas two doublets

Table IV. Structural Comparison of $[Fe_4O_2(O_2CCH_3)_7(bpy)_2]ClO_4)\cdot{}^1/_4CH_2Cl_2\cdot H_2O$ (**1**) with Other $[Fe_4O_2]^{8+}$ Molecules

	Distances (Å)					
	a	*b*	*c*	*d*	*e*	*f*
1	1.819	1.947	1.926	3.306	3.439	2.855
range	1.822–1.884	1.955–1.98	1.895–1.961	3.29–3.476	3.425–3.59	2.829–2.939

	Bond Angles (deg)			
	α	β	γ	δ
1	123.9	95.0	131.9	84.5
range	119.0–133.9	93.5–96.8	128.7–136.8	82.9–85.6

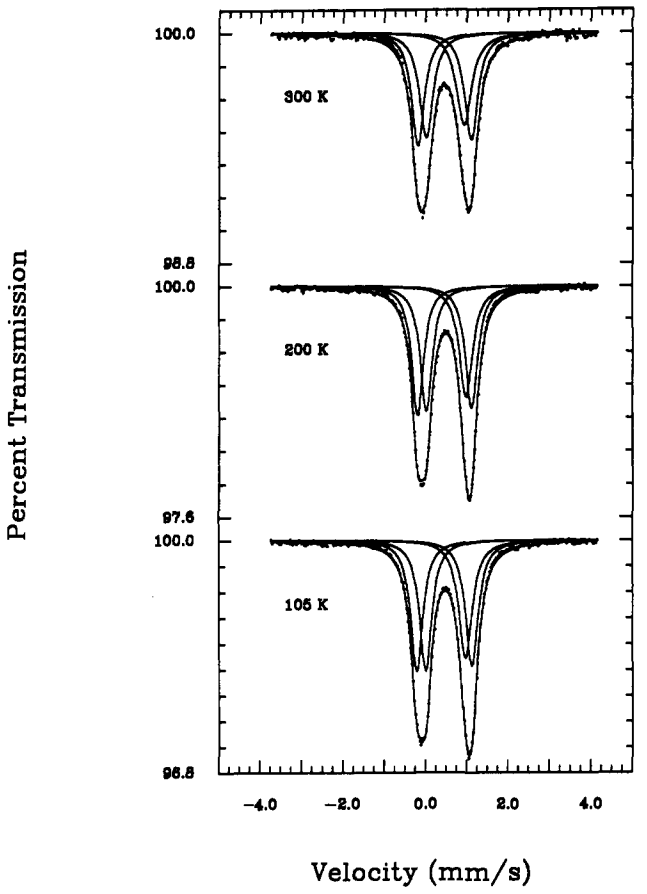

Figure 2. Variable-temperature ^{57}Fe Mössbauer spectrum for $[Fe_4O_2(O_2CCH_3)_7(bpy)_2](ClO_4)\cdot{}^1/_4CH_2Cl_2\cdot H_2O$ (**1**).

Table V. Mössbauer Fitting Parameters for $[Fe_4O_2(O_2CCH_3)_7(bpy)_2](ClO_4)\cdot{}^1/_4CH_2Cl_2\cdot H_2O$ (**1**)

T, K	ΔE_Q, mm/s	δ,[a] mm/s	Γ,[b] mm/s	−ln (area)[c]
300	1.293 (10)	0.459 (5)	0.185 (7), 0.199 (7)	−0.807 (11)
	0.916 (12)	0.472 (6)	0.226 (10), 0.196 (8)	
200	1.305 (5)	0.459 (2)	0.170 (3), 0.176 (3)	−0.062 (5)
	0.960 (6)	0.495 (3)	0.198 (5), 0.181 (4)	
105	1.333 (3)	0.457 (2)	0.177 (2), 0.178 (2)	0.267 (4)
	0.962 (4)	0.487 (2)	0.198 (3), 0.186 (3)	

[a] Isomer shift relative to iron foil at room temperature. [b] Full width at half height taken from least-squares fitting program. The width for the line at more negative velocity is listed first for each doublet. [c] Minus the natural logarithm of the background-normalized spectral area.

were seen for $[Fe_4O_2(O_2CCF_3)_8(H_2O)_6]\cdot 2H_2O$.[8c] In the latter complex the Fe–O_{oxo} bonds divide into two very distinct sets, with the closest approach between the two sets being 0.094 Å. For the former complex they found the various Fe–O distances form a more continuous set, with the closest approach being 0.041 Å. For our complex **1**, there are two quite distinct sets of Fe–O distances, and the closest approach between the two sets is 0.107 Å. Thus, it does seem that the principal distortion is due to the length of the Fe–(μ_3-oxo) bond.

^{1}H NMR Spectroscopy. An NMR investigation of complexes **1** and **3** has been carried out to complement that previously reported for the corresponding manganese complexes.[9,11b] In Figure 3 are shown the spectra recorded for these two iron complexes, together with that for the $CD_3CO_2^-$ version of **1**; the measured chemical shifts are tabulated in Table VI. The complexes are paramagnetic at the temperatures where the data were collected, and as a result the spectra consist of broad peaks that are shifted relative to their diamagnetic resonance positions. Nevertheless, all peaks were located, and the three spectra taken together allow for assignment of the various types of protons present. In addition, as will become evident from the following

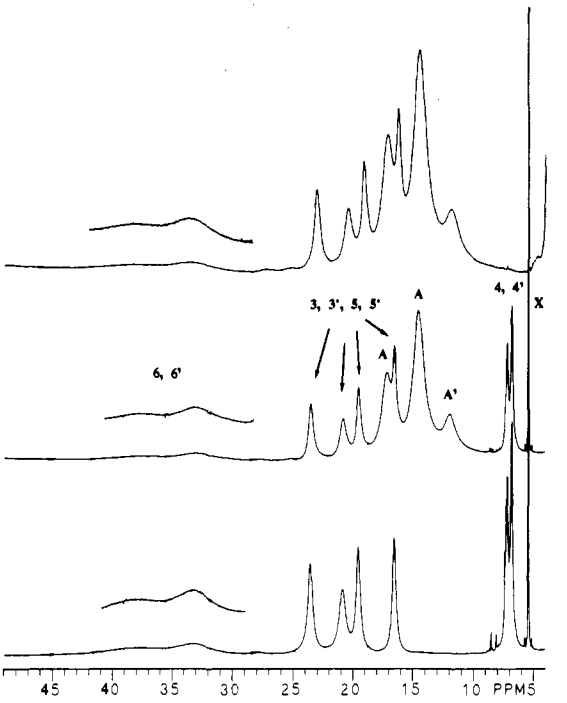

Figure 3. ^{1}H NMR spectra of complex **1** (middle), complex **3** (top), and the $CD_3CO_2^-$ analogue of complex **1** (bottom). See text for experimental details and assignment of resonances.

Table VI. ^{1}H NMR Data for Three $[Fe_4O_2]^{8+}$ Complexes in CD_3CN Solution at 23 °C

$[Fe_4O_2(O_2CR)_7(4,4'\text{-}X_2bpy)_2]^+$	ligand	shifts[a]
R = CH_3, X = H (**1**)	RCO_2^-	17.10, 14.51, 11.96[b]
	bpy[c]	37.70, 33.20 (6,6′)
		23.51, 20.81, 19.51, 16.50 (3,3′,5,5)
		7.22, 6.83 (4,4′)
R = CD_3, X = H	RCO_2^-	
	bpy[c]	37.75, 33.19 (6,6′)
		23.52, 20.83, 19.52, 16.49 (3,3′,5,5′)
		7.22, 6.83 (4,4′)
R = CH_3,	RCO_2^-	17.10, 14.46, 11.92[b]
X = Me (**3**)	bpy[c]	38.45, 33.93 (6,6′)
		23.09, 20.46, 19.08, 16.18 (3,3′,5,5′)
		3.84, 3.72 (4,4′Me)

[a] Data are chemical shifts in ppm (δ scale); downfield shifts are positive. [b] Unique acetate bridging the "body" Fe atoms. [c] Numbers in parentheses refer to the bpy ring positions.

discussion, the number of peaks present for cation **1** corresponds exactly to that expected based on the solid-state structure of the compound (C_2 site symmetry). This supports the notion that the complex retains its tetranuclear structure in MeCN solution. For the C_2 symmetry of complex **1**, four acetate peaks in a 2:2:2:1 integration ratio are expected. The three peaks marked A and A′ are clearly due to the acetate protons, since they are absent in the $CD_3CO_2^-$ analogue (Figure 3, bottom). The peak at 14.51 ppm likely arises from two overlapping peaks, consistent with its increased intensity. The peak at 11.96 ppm (A′) is assigned to the single, unique acetate group bridging the two central Fe atoms, Fe2 and Fe2′. The two A peaks correspond to the other six acetates.

In addition to the acetate peaks of **1**, there are eight additional peaks in the 5–40 ppm region, assignable to the bipyridine protons. Again, this is consistent with the presumed C_2 symmetry of the molecule. Consideration of peak widths allows for the assignment of the two very broad resonances at 37.70 and 33.20 ppm as being due to the 6,6′ protons, since they are closest to the metal centers. Along the same lines, the most peripheral bipyridine protons should give rise to the narrowest peaks; the peaks at 7.21 and 6.83 ppm are consequently assigned to the 4,4′ protons. This was confirmed by the absence of these resonances in the spectrum of the 4,4′-

Me_2bpy analogue, complex **3** (Figure 3, top), being replaced by the Me resonances at 3.84 and 3.72 ppm. The four remaining peaks are assigned to the 3,3′,5,5′ protons. These four peaks have similar widths, consistent with their near-equal distances from the nearest metal atom (4.346–4.458 Å), making specific assignments of these resonances difficult.

The spin–lattice relaxation times (T_1) of the cation protons in **1** were determined by the inversion recovery method. As expected due to the presence of the paramagnetic sites, the observed T_1 times are very short, on the order of 10^{-3} s. The A-type acetate protons exhibit T_1 times of 1.2–1.3 ms, whereas the A′ acetate protons show somewhat slower relaxation at 3.3 ms. The 4,4′-bpy protons exhibit the longest relaxation times, 6.0 and 7.1 ms for the 7.21- and 6.83-ppm peaks, respectively. The 3,3′,5,5′ protons gave values in the 2.5–3.9-ms range. Relaxation times for the 6,6′ protons could not be determined accurately due to the broadness of the resonances, but they clearly had the fastest T_1 times observed for complex **1** (<1 ms). The relative magnitudes of the relaxation times are inversely proportional to the observed peak widths and proportional to the distance of the protons from the nearest metal center.

Magnetochemistry. The magnetic susceptibility of complex **1** was measured at 10.0 kG in the range from 5.01–277.4 K. A plot of the effective moment per molecule versus temperature is given in Figure 4. The moment gradually decreases from 4.20 μ_B at 277.4 K to an essentially diamagnetic value of 0.82 μ_B at 5.01 K; the latter nonzero value is due to both temperature-independent paramagnetism (TIP) and an amount of a paramagnetic impurity (approximately 0.6%).[19] The data clearly indicate that this complex possesses an $S = 0$ ground state, in accord with what has been observed by Lippard and co-workers[7,8b] for molecules of similar structure. In a qualitative sense, the $S = 0$ state can be thought of in terms of an antiferromagnetic coupling of the four high-spin Fe(III) ions to produce a ground state of zero net spin. The gradual increase in the effective moment as the temperature is increased is obviously due to thermal population of spin states with $S > 0$.

As indicated earlier, the basic $[Fe_4O_2]^{8+}$ core structure of complex **1** is essentially identical with the so-called butterfly $[Mn_4O_2]^{n+}$ complexes we reported previously.[11] The magnetic exchange interactions in this system can be described in a similar fashion by use of the isotropic spin Hamiltonian given in eq 2

$$\mathbf{H} = -2J_{wb}(\mathbf{S}_1\cdot\mathbf{S}_2 + \mathbf{S}_2\cdot\mathbf{S}_{1'} + \mathbf{S}_{1'}\cdot\mathbf{S}_{2'} + \mathbf{S}_{2'}\cdot\mathbf{S}_1) - 2J_{bb}(\mathbf{S}_2\cdot\mathbf{S}_{2'}) \quad (2)$$

In this equation J_{wb} describes the "wing–body" exchange interactions about the periphery of the tetranuclear core, and J_{bb} describes the "body-body" or "hinge" interaction of the two central Fe(III) ions.[18] The numbering scheme for the $\mathbf{S}_i\cdot\mathbf{S}_j$ terms is that used in Figure 1. Defining $\mathbf{S}_A = \mathbf{S}_1 + \mathbf{S}_{1'}$, $\mathbf{S}_B = \mathbf{S}_2 + \mathbf{S}_{2'}$, and $\mathbf{S}_T = \mathbf{S}_A + \mathbf{S}_B$, equivalent-operator replacements can be made for all $\mathbf{S}_i\cdot\mathbf{S}_j$ terms in eq 2. The resulting eigenvalue eq 3

$$E = -J_{wb}[S_T(S_T + 1) - S_A(S_A + 1) - S_B(S_B + 1)] - J_{bb}[S_B(S_B + 1)] \quad (3)$$

was then used in the Van Vleck equation to derive an expression for the molar paramagnetic susceptibility of the complex.[20,21] For a system of four $S = {}^5/_2$ ions disposed in a butterfly-type arrangement, the overall degeneracy ($6^4 = 1296$) is distributed over 146 spin states with S values ranging from $S = 0$ to $S = 10$.

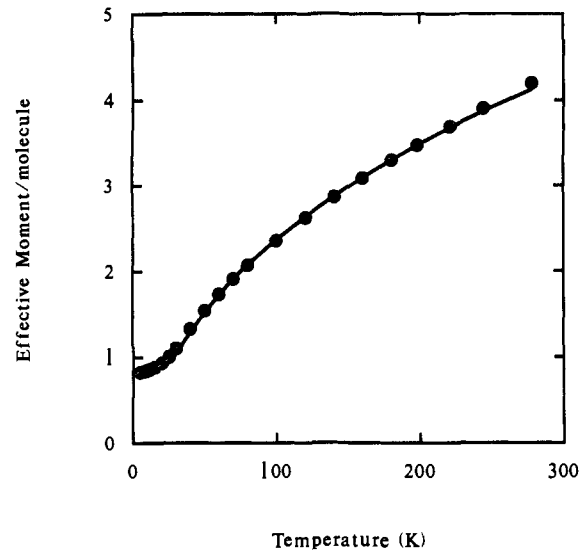

Figure 4. Plot of the effective moment of a polycrystalline sample of complex **1** as a function of temperature at 10.0 kG. The solid line represents a fit to the theoretical expression of the magnetic moment. See text for details.

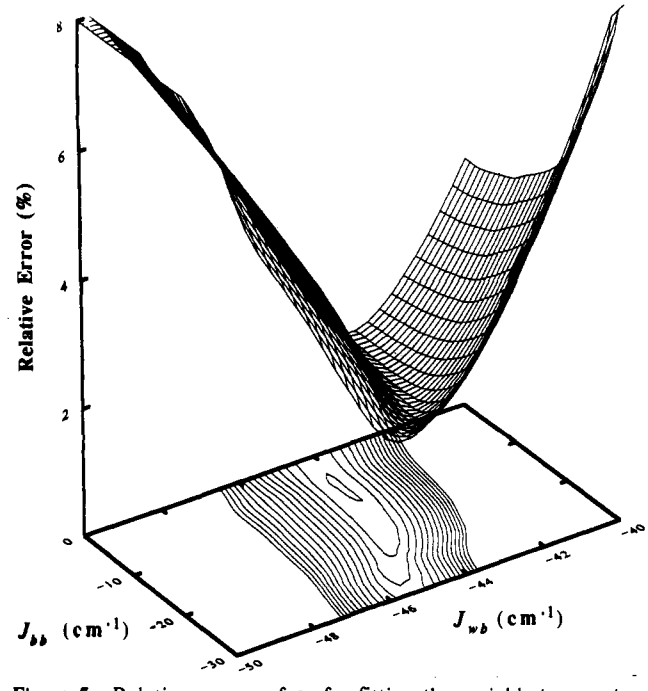

Figure 5. Relative error surface for fitting the variable-temperature magnetic susceptibility data of complex **1**. Only the region of parameter space which gives the smallest relative error is shown. The surface was calculated with $g = 2.00$, TIP = 800×10^{-6} cgsu, and 0.6% paramagnetic impurity held constant.

Results of Fitting: An Indeterminate J_{bb}. The susceptibility data for complex **1** were fit to the theoretical equation by means of an iterative relative-error minimization routine. The result of one such fit is indicated by the solid line in Figure 4. This fit gave parameters of $J_{wb} = -45.5$ and $J_{bb} = -8.9$ cm^{-1}, with g, TIP, and weight percent paramagnetic impurity fixed at 2.00, 800×10^{-6} cgsu, and 0.6, respectively. It is clear that the theoretical curve fits the experimental data quite well. To determine if this

(12) Cohn, M. J.; Timken, M. D.; Hendrickson, D. N. *J. Am. Chem. Soc.* **1984**, *106*, 6683.
(13) Chrisman, B. L.; Tumolillo, T. A. *Comput. Phys. Commun.* **1971**, *2*, 322.
(14) *Theory and Applications of Molecular Paramagnetism*; Boudreaux, E. A., Mulay, L. N., Eds.; John Wiley and Sons, Inc.: New York, 1976.
(15) Schmitt, E. A., unpublished results.
(16) Chisholm, M. H.; Folting, K.; Huffman, J. C.; Kirkpatrick, C. C. *Inorg. Chem.* **1984**, *23*, 1021.
(17) Khedekar, A. V.; Lewis, J.; Mabbs, F. E.; Weigold, H. *J. Chem. Soc. A* **1967**, 1561.
(18) For comparative purposes, J_{wb} and J_{bb} correspond to J and J_{13}, respectively, for the equations used in analyzing the analogous manganese complexes.[11a]
(19) The paramagnetic impurity was incorporated as a mole percent contribution of an $S = 5/2$ species added to the calculated susceptibility.
(20) Van Vleck, J. H. *Electric and Magnetic Susceptibilities*; Oxford University Press: Oxford and New York, 1932.
(21) The complete expression in J_{bb} involves terms for S_2 and $S_{2'}$. Since these terms are constants for the system, they have been omitted from eq 3.

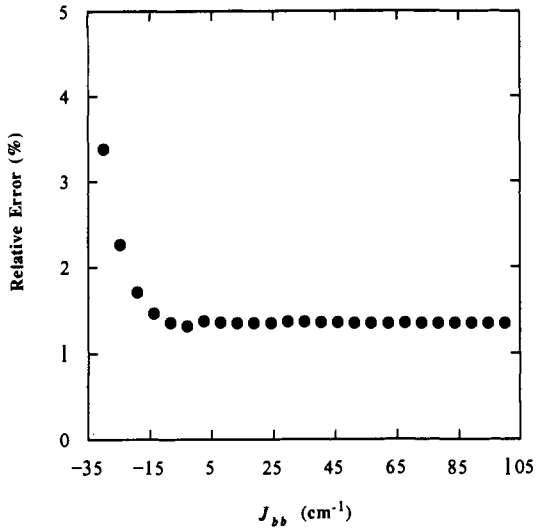

Figure 6. Plot of the relative fitting error for complex **1** as a function of J_{bb}. The value of J_{wb} was held fixed at -45 cm^{-1}.

fit was unique, a search of all four quadrants of (J_{wb},J_{bb}) parameter space was performed. Figure 5 summarizes the results of this search in the form of a relative error surface for fitting of the data to theoretical expression (only the region of smallest relative error is represented in the figure). These calculations indicate a well-defined minimum in J_{wb} about -45 cm^{-1}, consistent with the least-squares fit. This value is also consistent with the empirical correlations which have been made regarding Fe–$O_{\mu\text{-oxo}}$ bond lengths and the strength of magnetic exchange interactions in other polynuclear ferric complexes.[1a,10] The Fe1–O3 bond length of 1.819 (5) Å in complex **1** is intermediate between what is considered a "short" Fe–$O_{\mu\text{-oxo}}$ distance of ca. 1.78–1.79 Å ($J \approx -120$ cm^{-1}) and a "long" Fe–$O_{\mu\text{-oxo}}$ distance ($d \approx 1.95$–1.96 Å, $J \approx -20$ cm^{-1}) observed for several oxo-bridged binuclear Fe(III) complexes. It has been observed experimentally that perturbation of oxo bridges in diiron systems (e.g., protonation or metal binding) substantially reduces the strength of the exchange interaction, so the relatively small value of J_{wb} given the Fe–$O_{\mu\text{-oxo}}$ bond distance is not surprising.[1a,10] The observed value of J_{wb} for complex **1** does fall in the range which has been observed for trinuclear iron acetates,[22] lending some credibility to the formulation of these $[Fe_4O_2]^{8+}$ complexes as edge-sharing μ_3-O trinuclear fragments.

However, the minimum in J_{bb} is much less well-defined; this is apparent in Figure 6 which gives a plot of relative error versus J_{bb} for $J_{wb} = -45$ cm^{-1} (g, TIP, and percent of impurity were fixed as before). The relative error for fitting the magnetic data is essentially unaffected for J_{bb} ranging from -15 cm^{-1} to a value in excess of $+100$ cm^{-1}, with a very shallow minimum at about $J_{bb} = -10$ cm^{-1}. Figure 7 illustrates this with actual fits of the effective moment for complex **1** at three different points along the isoerror line ($J_{wb} = -45$ cm^{-1}) for $J_{bb} = -10$, $+50$, and $+100$ cm^{-1}. The data are equally well fit regardless of the value of $J_{bb} > -15$ cm^{-1}. To ensure that this remarkable insensitivity to J_{bb} was something intrinsic in the $[Fe_4O_2]^{8+}$ system and not specific for complex **1**, a similar analysis was carried out on another compound already in the literature. Lippard et al.[7] reported the effective moment data as a function of temperature for $(Et_4N)[Fe_4O_2(O_2CPh)_7(H_2B(pz)_2)_2]$. The relative error surface for fitting of these data is given in Figure 8. Clearly, the same situation is encountered for this system: a well-defined minimum is found for J_{wb} centered around -42 cm^{-1}, but no such minimum can be found for J_{bb}.

Mathematical vs Physical Origin of J_{bb} Dependence: Molecular Spin Frustration. The indeterminate nature of the J_{bb} interaction in the $[Fe_4O_2]^{8+}$ core was surprising to find. It has already been well-established by Lippard and others[1a,22] that exchange interactions for high-spin Fe(III) ions bridged by O^{2-} or OR^- are overwhelmingly antiferromagnetic in nature. The strength of the interaction has been found to be essentially a function of Fe–O bond distance only,[10] since the isotropic d-electron distribution of a high-spin d^5 ion eliminates any angular dependence. Only for one complex has a very weak ferromagnetic interaction been noted.[23] Why should a *ferromagnetic* interaction apparently describe body–body magnetic characteristics of these $[Fe_4O_2]^{8+}$ complexes? There are two ways to answer this question, and we shall examine each in detail.

The first is strictly mathematical in nature. Examination of the theoretical curves in Figures 6 and 7 shows that changing the value of J_{bb} has absolutely no effect on the magnetic susceptibility of complex **1**. This is, of course, very counterintuitive; the ions involved in the J_{bb} interaction (Fe2 and Fe2′) do not function independently, since they are also interacting with the two wing-tip ions Fe1 and Fe1′. Changing the strength of the Fe2···Fe2′ interaction should affect the J_{wb} parameter, and therefore should consequently affect the overall magnetic structure of the complex. This is, in fact, true in the $[Fe_4O_2]^{8+}$ system. However, *a change in the magnetic susceptibility in response to a change in J_{bb} is only manifested in the higher lying magnetic states, not in the states that are thermally populated at 300 K.* This is illustrated in Figure 9, which shows the energies of the states of complex **1** for $J_{wb} = -45$ cm^{-1} with $J_{bb} = -10$, $+50$, or $+100$ cm^{-1}. With the exception of an $S = 1$ state at 440 cm^{-1} for the $J_{bb} = -10$-cm^{-1} case, the excited spin-state distributions for all three descriptions are identical up to energies 540 cm^{-1} above the ground state. There are differences among the three descriptions which become apparent for energy levels which are higher in energy than 540 cm^{-1}. In general, a larger positive J_{bb} tends to stabilize more states of larger S value, consistent with what one would expect on increasing the magnitude of a ferromagnetic interaction. However, none of these higher excited states contribute significantly to the magnetic susceptibility of the complex in the 5–300 K region where the data were collected. In essence then, the insensitivity of fitting the data for the $[Fe_4O_2]^{8+}$ complex to the value of J_{bb} is due to the fact that data measured up to 300 K are simply not sufficient to discriminate and establish the J_{bb} dependence. Only if the susceptibility data were measured at very high temperatures would it be possible to determine the value of J_{bb}. The thermal stabilities of these complexes (ClO_4^- salts) do not permit measurements at much higher temperatures.

The above discussion serves to explain the mathematics behind the theoretical analysis but does little to shed light on the physical origin of the apparent lack of a J_{bb} dependence. After all, regardless of how the excited-state distribution changes, we are still left with the fact that the exchange interaction between the two central Fe(III) ions can vary from being weakly antiferromagnetic to strongly *ferromagnetic* without changing the magnetic ground and low-lying excited states of the molecule. To understand the physical origin of this, we must look to the vector coupling which produces the lowest lying magnetic states of the complex.

The strongest antiferromagnetic *pairwise* interaction in complex **1** occurs between one wing-tip ion [Fe(1) or Fe(1′)] and one of the body iron ions [Fe(2) or Fe(2′)]. This was established in the above data analysis. It is easly to see, however, that this causes a "spin frustration" relative to the Fe(2)···Fe(2′) interaction. This can be seen by focusing on the Fe(1)···Fe(2) interaction. An antiparallel spin alignment on these two iron ions can be pictorially represented as follows.

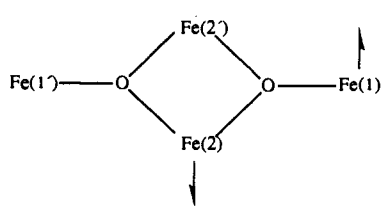

(22) Cannon, R. D.; White, R. P. *Prog. Inorg. Chem.* **1988**, 36.

(23) An extremely weak ferromagnetic interaction has been observed very recently in a binuclear ferric complex, see: Snyder, B. S.; Patterson, G. S.; Abrahamson, A. J.; Holm, R. H. *J. Am. Chem. Soc.* **1989**, *111*, 5214.

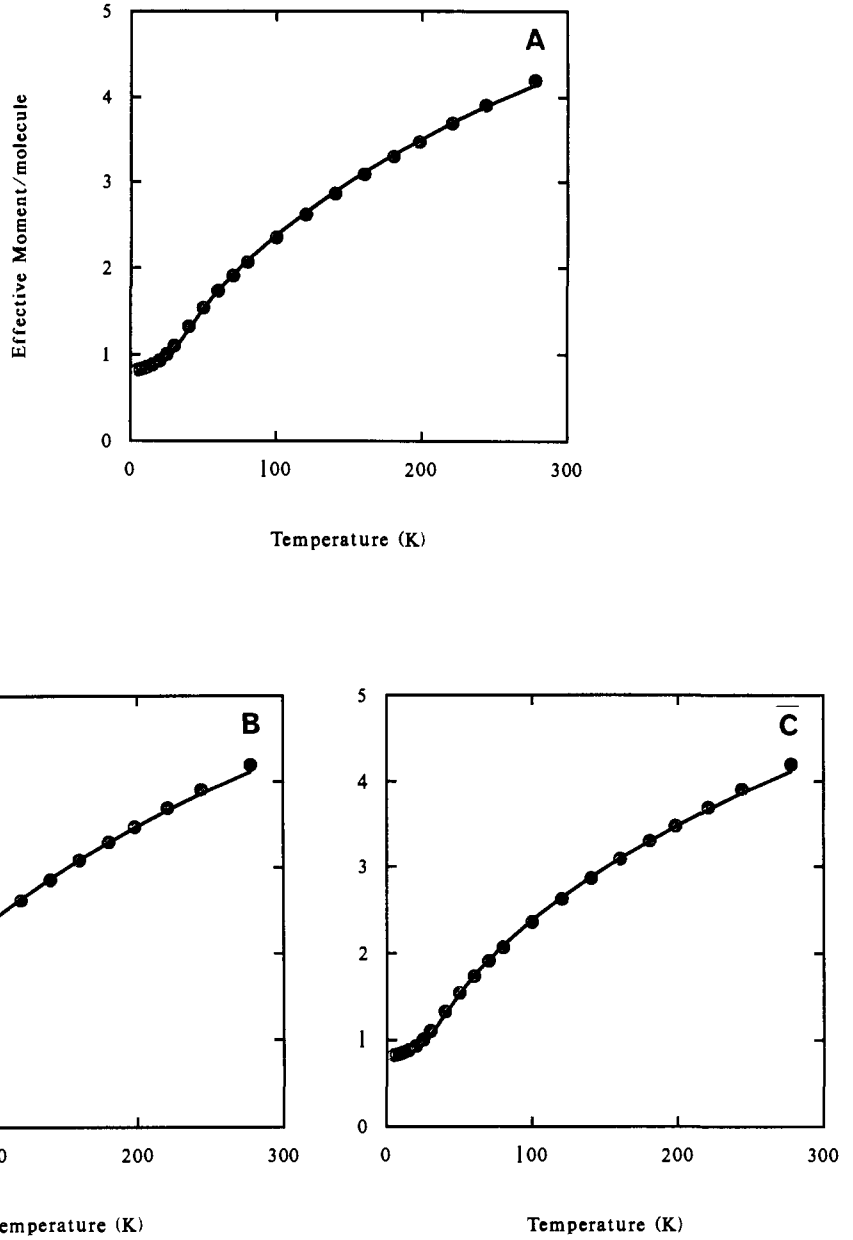

Figure 7. Plots of theoretical effective moment vs temperature curves (solid lines) for $J_{wb} = -45$ cm^{-1} with $J_{bb} = -10$ cm^{-1} (A), +50 cm^{-1} (B), or +100 cm^{-1} (C). The experimental data for complex **1** are shown as filled circles.

Since the Fe(1)···Fe(2′) and Fe(1)···Fe(2) interactions are equal, the spin alignment on the Fe(2′) ion also tends to be antiparallel to that on the Fe(1) ion. This means, of course, that the spins on Fe(2) and Fe(2′) will tend to be parallel (ferromagnetic interaction). Thus, if the Fe(1)···Fe(2) [≡Fe(1)···Fe(2′)] interaction is antiferromagnetically greater than the Fe(2)···Fe(2′) interaction, the overall favored spin alignment is as follows.

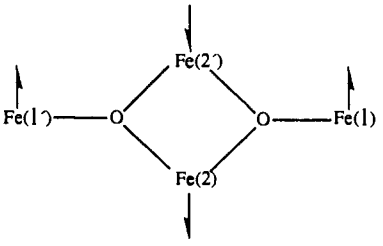

The net result of the above spin alignments is a ground state with $S_T = 0$. There are, in fact, six spin states of the $[Fe_4O_2]^{8+}$ complex which have $S_T = 0$. For each of these six $S_T = 0$ states $S_A = S_B$. It takes only a little thought to realize that the most stable $S_T = 0$ ground state comes about when S_A and S_B each have their maximum values of $S_A = S_B = 5$. The vector coupling of $S_A = 5$ and $S_B = 5$ gives rise to a range of states where $S_T = 0, 1, 2, \ldots 10$. An examination of the eigenstates illustrated in Figure 9 reveals that not only is this $S_T = 0$ state the ground state, but the $S_T = 1$ and $S_T = 2$ states which come from vector coupling of $S_A = 5$ and $S_B = 5$ are the two lowest energy excited states. The Fe(2)···Fe(2′) interaction is thus frustrated: it cannot be more antiferromagnetic than the Fe(1)···Fe(2) interaction and maintain the integrity of the low-lying spin states. However, since a ferromagnetic Fe(2)···Fe(2′) interaction in fact stabilizes the magnetic states which are populated at room temperature, the theoretical analysis is accommodated by a wide range of J_{bb} values, provided that J_{bb} is not strongly antiferromagnetic. It is in this manner that J_{bb} becomes indeterminate.

It is important to clarify precisely what we mean by spin frustration in this system. To do this, it is instructive to compare the magnetic exchange interactions present in complex **1** to those present in the analogous complex $[Mn_4O_2(O_2CCH_3)_7(bpy)_2](ClO_4)$. A detailed analysis[11b] of the data for this Mn_4^{III} complex gave $J_{wb} = -7.8$ and $J_{bb} = -23.5$ cm^{-1}. In this instance, the body–body interaction is dominant. However, unlike the Fe_4^{III} complex, the Mn_4^{III} complex has an extremely complicted low-

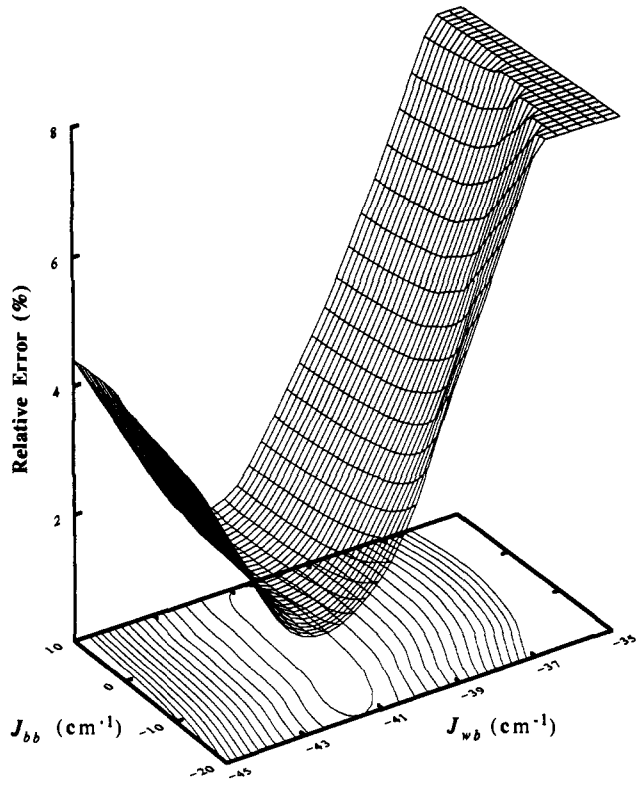

Figure 8. Relative error surface for fitting of magnetic susceptibility data for $(Et_4N)[Fe_4O_2(O_2CPh)_7(H_2B(pz)_2)_2]$. Data were taken from ref 7. The surface was calculated with $g = 2.00$, TIP = 800×10^{-6} cgsu, and 0.06% of a $S = 5/2$ paramagnetic impurity.

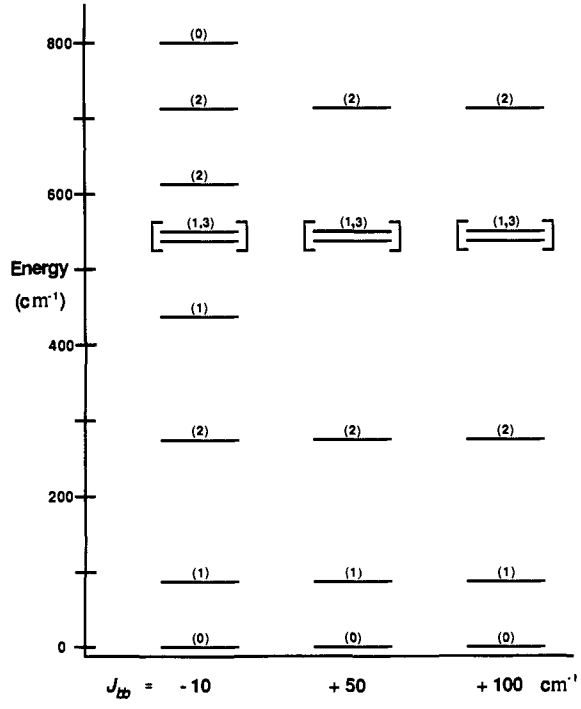

Figure 9. Calculated eigenvalues of lowest energy states for complex **1** for $J_{wb} = -45$ cm^{-1} as a function of J_{bb}. The numbers in parentheses indicate the value of S_T for each state. The energy of the $S_T = 0$ ground state has arbitrarily been set at 0 cm^{-1}.

lying magnetic structure with an intermediate spin ground state of $S_T = 3$ and six low-lying excited states within 30 cm^{-1}, ranging from $S_T = 0$ to $S_T = 4$. The $S_T = 3$ ground state results from an antiferromagnetic alignment of the vector-coupled terms $S_A = 4$ and $S_B = 1$. Thus, the relatively strong body–body antiferromagnetic interaction does tend to pair up the spins on Mn(2) and Mn(2′). However, the resultant of that spin–spin interaction is not $S_B = 0$ but rather $S_B = 1$. The body–body interaction is frustrated in this case, producing an intermediate vector-coupled state due to the fact that each of the body Mn^{III} ions is also antiferromagnetically coupled to a wing-tip Mn^{III} ion. The origin of the frustration is linked to the ratio for the two J values. In the case of the Mn_4^{III} complex, $J_{wb}/J_{bb} \simeq 0.33$. It is this ratio of the two coupling constants that gives rise to the $S_B = 1$ state and the complex magnetic structure of the Mn_4^{III} compound.

Now let us examine the magnetic structure of **1**. The eigenstates in Figure 9 indicate that the ground state in this complex is well isolated. Moreover, the vector coupling giving rise to the ground and low-lying excited states represents an *extreme* coupling situation (i.e., both S_A and S_B are at their maximum values of 5), in contrast with the intermediate situation of $S_B = 1$ found in the Mn_4^{III} complex. The ratio J_{wb}/J_{bb} for complex **1** based on the above analysis is not less than about 3. The spin frustration present in the Fe_4^{III} case, then, represents an extreme situation where one interaction (J_{wb}) dominates the other to the extent that the intrinsic character of the J_{bb} interaction is totally negated. We believe that the Fe(2)···Fe(2′) interaction is likely antiferromagnetic in nature. However, the strength of the J_{wb} interaction relative to the J_{bb} interaction is such that the natural tendency for the spin vectors on Fe(2) and Fe(2′) to align antiparallel is overcome. The result is a ferromagnetic alignment of the Fe(2)···Fe(2′) spin vectors and a frustration of that spin–spin interaction.

Spin frustration is a well-known phenomenon for several extended lattices involved in magnetic exchange interactions.[24] For example, consider a lattice made up of equilateral triangles of $S = 1/2$ metal ions. If all three metal ions in a triangle are equivalent and the pairwise magnetic exchange interaction is antiferromagnetic, then frustration develops. In other words, if the A and B metal ions are involved in an antiferromagnetic interaction in the triangle below, then what spin should the C metal ion assume? In the above $[Fe_4O_2]^{8+}$ complexes, this same type of frustration is present.

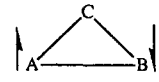

Concluding Comments

Spin frustration is present in $[Fe_4O_2(O_2CCH_3)_7(bpy)_2](ClO_4)$, which has a butterfly core. In this Fe_4^{III} complex it has been found that the wing-tip–body [e.g., Fe(1)···Fe(2)] antiferromagnetic interaction is greater than the body–body [Fe(2)···Fe(2′)] antiferromagnetic interaction. For the former $J_{wb} = -45$ cm^{-1} and for the latter $J_{bb} > -15$ cm^{-1}. The Fe(1)···Fe(2) type interaction is more antiferromagnetic due to the fact that the Fe(1)–O(3)–Fe(2) exchange pathway includes one short [Fe(1)–O(3) = 1.819 (5) Å] and one long [Fe(2)–O(3)] = 1.926 (5) Å] bond distance. The body–body exchange pathway, Fe(2)–O(3)–Fe(2′), has two of the longer Fe–O(oxide) bond lengths. Since J_{wb} is appreciably more negative than J_{bb}, there is frustration in the spin alignment associated with the two body iron ions, causing an intrinsically antiferromagnetic spin interaction to tend to be ferromagnetic. A $S_T = 0$ ground state is found which results from a vectorial coupling of the $S_A = 5$ coupled spin of the two wing-tip iron ions with the $S_B = 5$ coupled spin of the two body iron ions. The energies of this $S_T = 0$ ground state and all thermally populated excited states are effectively only determined by J_{wb}. The value of J_{bb} is poorly defined and only can be said to be more positive than -15 cm^{-1}.

The relatively weak nature of the antiferromagnetic interactions observed for complex **1** and one other $[Fe_4O_2]^{8+}$ complex is notable. For a large number of $Fe^{III}(\mu\text{-}O)_2Fe^{III}$ complexes the antiferromagnetic interaction is characterized by $J = -100$ to -150 cm^{-1}.

(24) Ghose, S.; Hewat, A. W.; Pinkney, M. *Solid State Commun.* **1990**, *74*, 413–418, and references therein.
(25) Shiemke, A. K.; Loehr, T. M.; Sanders-Loehr, J. *J. Am. Chem. Soc.* **1986**, *108*, 2437 and references cited therein.

Protonation of the oxide bridge is known to reduce the magnitude of the antiferromagnetic interaction. For example, protonation of the oxide bridge in $[(HB(pz)_3Fe)_2O(OAc)_2]$ to give $[(HB(pz)_3Fe)_2(OH)(OAc)_2]^+$ changes J from -121 to $J = -17$ cm^{-1}. The Fe–O bond distance also increases from 1.784 to 1.956 Å.[1a] In fact, hydrogen-bonding contacts involving an oxide bridge between two Fe^{III} ions have been suggested for proteins with binuclear iron sites.[1a,c,25] In the case of oxyhemerythrin (oxy-Hr) a hydroperoxide ($O-O-H^-$) ligand coordinated to one Fe^{III} ion is believed to be involved in a hydrogen-bonding contact interaction with the oxide bridge. For oxyHr a J value of -77 cm^{-1} is found, which is to be compared to -134 cm^{-1} for Fe_2^{III} metHr. A hydrogen-bonding contact interaction has also been suggested for the $\overset{\lceil O \rceil}{Fe^{III}Fe^{III}}$ bridge in the ribonucleotide reductase from *E. coli*.

Acknowledgment. This work was supported by the NIH Grant HL13652 to D.N.H. and the NSF Grant CHE8808019 to G.C.

Supplementary Material Available: Complete listings of bond distances and angles, anisotropic thermal parameters, and magnetic susceptibility data for $[Fe_4O_2(O_2CCH_3)_7(bpy)_2](ClO_4)\cdot {}^1/_4CH_2Cl_2\cdot H_2O$ (**1**) (6 pages); tables of observed and calculated structure factors (8 pages). Ordering information is given on any current masthead page. A complete structure report for complex **1** (No. 88019) is available upon request from the Indiana University Chemistry Library.

Heteronuclear ^{13}C–^1H NMR Investigation of the Effects on an Oligodeoxyribonucleotide of Intrastrand Cross-Linking by a Pt Anticancer Drug. A Large Shift of C3′ Accompanies an S to N Conformational Change

Srinivasan Mukundan, Jr.,[†] Yinghai Xu,[†] Gerald Zon,[‡] and Luigi G. Marzilli*,[†]

Contribution from the Department of Chemistry, Emory University, Atlanta, Georgia 30322, and Applied Biosystems, Foster City, California 94404. *Received September 4, 1990*

Abstract: NMR spectral characterization of DNA and RNA oligonucleotides with unusual structural features may be impeded by the absence of NOE connectivities in the 2D homonuclear proton NOESY spectrum. Furthermore, in larger oligonucleotides, signal overlap may prevent an accurate measurement of the homonuclear coupling constants necessary to assess average sugar conformation. As part of an ongoing study of the effects of platinum anticancer drugs on deoxyribonucleotides, we examined the use of ^{13}C NMR spectroscopy on the model systems, $d(T_1G_2G_3T_4)$ and $[d(T_1G_2G_3T_4)N7,N7]$-Pt(en), where en = ethylenediamine and the N7 of both G's is attached to the metal. Such an intrastrand cross-link adduct is the major lesion formed when such anticancer drugs bind to DNA. These oligonucleotides were examined with both heteronuclear multiple-quantum coherence (HMQC) and heteronuclear multiple-bond correlation (HMBC) spectroscopy. Intranucleotide heteronuclear scalar connectivities were observed between the H1′ and the pyrimidine base C2 and C6 signals and the pyrimidine H6 and deoxyribose C1′ signals, thereby circumventing the need to rely on the less certain NOE connectivities to identify the base and sugar signals of the same nucleotide. For the parent oligonucleotide, a similar set of heteronuclear couplings was observed for the H1′, C8, and C4 signals of the purine nucleotides. However, for $[d(T_1G_2G_3T_4)$-$N7,N7]$-Pt(en), these latter connectivities were not observed, a result consistent with a structural distortion caused by platination. Nevertheless, the purine base ^{13}C signals gave the characteristic pattern of shift changes expected for N7 metalation predicted on the basis of past studies on mononucleotides. The method should be useful in identifying metalation sites in oligonucleotides. Comparison of solid-state ^{13}C data for deoxyribose moieties in the N and the S conformations leads to the prediction that the ^{13}C signals will undergo appreciable shift changes in any transformation that induces an S to N conformational change. We found that, at 12 °C, the C3′ signal of G_2 in $d(T_1G_2G_3T_4)$ was shifted upfield by 6.6 ppm in $[d(T_1G_2G_3T_4)$-$N7,N7]$-Pt(en), consistent with such a conformational change. Of considerable interest, the H1′ signal of G_2 $[d(T_1G_2G_3T_4)$-$N7,N7]$-Pt(en) was broad at 12 °C; it shifted downfield and sharpened with an increase in temperature to 40 °C. No appreciable changes were observed in the ^{13}C shifts, suggesting that the characteristic behavior of the H1′ signal of the 5′G in such cross-links is not the result of a significant change in the average conformation of the deoxyribose moiety but may be due to changes in the orientation of the bases with respect to the deoxyribose and/or the Pt coordination sphere.

Introduction

Modern 2D NMR spectroscopy is gaining ever-increasing application to the study of biomolecules.[1] NMR studies of oligonucleotides can provide insight into unusual structures present in DNA or RNA, such as hairpins and bulges, or novel structures formed by the treatment of DNA with anticancer drugs or intercalators.[2-9] Most studies have utilized ^1H NMR spectroscopy, while fewer studies have examined other nuclei, particularly ^{31}P.[9] Although ^1H NMR spectra of regular duplex DNA structures can be assigned with little difficulty, conformationally flexible structures, such as single-stranded DNA or those induced by anticancer compounds, may not have all the necessary ^1H–^1H NOE cross peaks for sequential assignments.[5] Increased emphasis is now being placed on ^{13}C NMR spectroscopy of oligonucleotides

[†] Emory University.
[‡] Applied Biosystems.

(1) Wüthrich, K. *NMR of Proteins and Nucleic Acids*; John Wiley & Sons: New York, 1986. See also: Live, D., Armitage, I. M., Patel, D., Eds. *Frontiers of NMR in Molecular Biology*; Wiley-Liss: New York, 1990.
(2) Wemmer, D. E.; Chou, S. H.; Hare, D. R.; Reid, B. R. *Nucleic Acids Res.* **1985**, *13*, 3755. Hare, D. R.; Reid, B. R. *Biochemistry* **1986**, *25*, 5341. Ikuta, S.; Chattopadhyaya, R.; Ito, H.; Dickerson, R. E.; Kearns, D. R. *Biochemistry* **1986**, *25*, 4840. Orbons, L. P. M.; van Beuzekom, A. A.; Altona, C. *J. Biomol. Struct. Dyn.* **1987**, *4*, 965. Summers, M. F.; Byrd, R. A.; Gallo, K. A.; Samson, C. J.; Zon, G.; Egan, W. *Nucleic Acids Res.* **1985**, *13*, 6375.
(3) Roy, S.; Sklenar, V.; Appella, E.; Cohen, J. S. *Biopolymers* **1987**, *26*, 2041. Nikonowicz, E. P.; Meadows, R. P.; Gorenstein, D. G. *Biochemistry* **1990**, *29*, 4193. Hare, D.; Shapiro, L.; Patel, D. J. *Biochemistry* **1986**, *25*, 7456. van den Hoogen, Y. Th.; van Beuzekom, A. A.; de Vroom, E.; van der Marel, A.; van Boom, J. H.; Altona, C. *Nucleic Acids Res.* **1988**, *16*, 5013.

0002-7863/91/1513-3021$02.50/0